Phase correction for a distorted orbital angular momentum beam using a Zernike polynomials-based stochastic-parallel-gradient-descent algorithm

Guodong Xie,[1,*] Yongxiong Ren,[1] Hao Huang,[1] Martin P. J. Lavery,[2] Nisar Ahmed,[1] Yan Yan,[1] Changjing Bao,[1] Long Li,[1] Zhe Zhao,[1] Yinwen Cao,[1] Moshe Willner,[1] Moshe Tur,[3] Samuel J. Dolinar,[4] Robert W. Boyd,[2,5,6] Jeffrey H. Shapiro,[7] and Alan E. Willner[1]

[1]*Department of Electrical Engineering, University of Southern California, Los Angeles, California 90089, USA*

[2]*School of Physics and Astronomy, University of Glasgow, Glasgow G12 8QQ, UK*

[3]*School of Electrical Engineering, Tel Aviv University, Ramat Aviv 69978, Israel*

[4]*Jet Propulsion Laboratory, California Institute of Technology, Pasadena, California 91109, USA*

[5]*Department of Physics and Astronomy, The Institute of Optics, University of Rochester, Rochester, New York 14627, USA*

[6]*Department of Physics, University of Ottawa, 150 Louis Pasteur, Ottawa, Ontario K1N 6N5, Canada*

[7]*Research Laboratory of Electronics, Massachusetts Institute of Technology, Cambridge, Massachusetts 02139, USA*

**Corresponding author: guodongx@usc.edu*

Received December 23, 2014; revised February 10, 2015; accepted February 15, 2015;
posted February 18, 2015 (Doc. ID 231341); published March 17, 2015

A stochastic-parallel-gradient-descent algorithm (SPGD) based on Zernike polynomials is proposed to generate the phase correction pattern for a distorted orbital angular momentum (OAM) beam. The Zernike-polynomial coefficients for the correction pattern are obtained by monitoring the intensity profile of the distorted OAM beam through an iteration-based feedback loop. We implement this scheme and experimentally show that the proposed approach improves the quality of the turbulence-distorted OAM beam. Moreover, we apply phase correction patterns derived from a probe OAM beam through emulated turbulence to correct other OAM beams transmitted through the same turbulence. Our experimental results show that the patterns derived this way simultaneously correct multiple OAM beams propagating through the same turbulence, and the crosstalk among these modes is reduced by more than 5 dB.

OCIS codes: (010.1330) Atmospheric turbulence; (010.1285) Atmospheric correction; (060.4230) Multiplexing.
http://dx.doi.org/10.1364/OL.40.001197

Orbital angular momentum (OAM) multiplexing has emerged as an optical communication technique for the simultaneous transmission of spatially overlapping orthogonal modes that can be efficiently multiplexed at the transmitter and demultiplexed at the receiver [1,2]. A light beam with a helical phase front of the form $\exp(i\ell\theta)$ carries OAM, where the integer ℓ is the OAM topological charge and θ is the azimuthal angle [3–5]. OAM beams with different ℓ values are orthogonal to one another. Terabit/s data transmissions using OAM multiplexing over short free-space ranges have been demonstrated with little distortion imposed by the propagation [2,6]. However, the beams in a practical free-space link may be distorted during propagation because of factors such as atmospheric turbulence [7–12]. In such cases phase-front distortions can severely degrade demultiplexing performance, motivating attempts to apply phase-front correction prior to demultiplexing.

A critical challenge for phase-front correction is characterizing the wavefront distortion incurred on each OAM beam [7–12]. OAM beams with $\ell \neq 0$ have a helical phase structure with a phase and power singularity at beam center. Standard wavefront sensors, such as the Shack–Hartmann, rely on intensity differentials between parts of a received beam to calculate the distortion [13,14]; this power singularity may cause compensation systems using these traditional sensors to fail [15].

Recently, turbulence compensation for a free-space OAM multiplexed system has been demonstrated in a system that used a Shack–Hartmann sensor to measure the wavefront distortion on a Gaussian beam ($\ell = 0$) that co-propagated with, but was polarized orthogonally to, the OAM communication beams [16]. It might be desirable to design a sensing method whose probe beam could have a phase singularity (e.g., an OAM beam with $\ell \neq 0$) such that the probe beam would spatially overlap with the information carrying beams during propagation.

Rather than measuring the phase of the incoming distorted OAM beam, we propose to use its intensity pattern, together with a Zernike-polynomials-based stochastic-parallel-gradient-descent (SPGD) algorithm [13,14,17–19] to derive the phase correction pattern (in [20], intensity profile monitoring was employed to recognize the order of the distorted OAM beams, but the distortion was not finally corrected). The resulting phase correction pattern can efficiently remove a significant part of the acquired distortion on the probe beam (see Fig. 1). In addition, this pattern can be used as the phase correction of other OAM beams that passed through the same distorting transmission medium.

A two-dimensional phase pattern on the unit disk can be approximated, in polar coordinates, by a linear

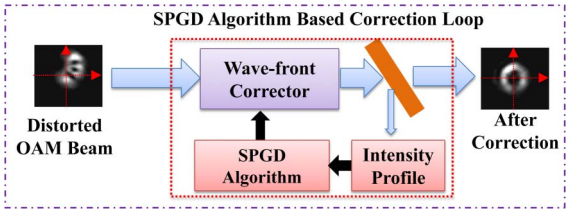

Fig. 1. Concept of phase correction for a distorted OAM beam. SPGD, stochastic parallel gradient descent.

combination of orthogonal Zernike polynomials $Z_n(r,\theta)$ as [21–23]

$$\varphi(r,\theta,a_1,a_2,\ldots,a_N)=\sum_{n=1}^{N}a_nZ_n(r,\theta),\quad 0\le r\le 1,\quad 0\le\theta\le 2\pi. \tag{1}$$

Here, a_n is the coefficient of the nth Zernike polynomial and N is the number of terms (up to 14 terms in our experiment) in the approximation. Thus the critical step in deriving a correction pattern for a distorted OAM beam is to determine the coefficients of Zernike polynomial in a fast and accurate way. The proposed SPGD algorithm for determining these coefficients is as follows:

Feedback signals: As shown in [24], the mode purity of an OAM beam increases monotonically with increasing quality of its intensity profile, which is defined as correlation coefficient C_k between the far-field intensity profile of the OAM beam $I(r,\theta)$ and its ideal intensity distribution $I_{\mathrm{id}}(r,\theta)$, namely,

$$C_k=\int_0^1\int_{-\pi}^{\pi}I(r,\theta)I_{\mathrm{id}}(r,\theta)\mathrm{d}\theta\mathrm{d}r. \tag{2}$$

The higher the correlation coefficient, the closer the measured OAM beam is to its unperturbed shape. This suggests that the intensity profile can be used to derive the error signal in the feedback loop to update the correction phase pattern.

Initialization: The algorithm starts with a blank correction pattern: $\varphi_0=\varphi(r,\theta,0,0,\ldots,0)$.

Correction-pattern iteration: Given the kth ($k\ge 0$) iteration, the process for the $(k+1)$th iteration of the algorithm is shown in Fig. 2. First, the current correction pattern, $\phi_k(r,\theta)=\phi(r,\theta,a_{1,k},a_{2,k},\ldots,a_{N,k})$, is used to partially restore the OAM beam's wavefront, and the intensity profile of the partially restored beam $I_{1,k}(r,\theta)$ is recorded. The correlation coefficient $C_{1,k}$ between $I_{1,k}(r,\theta)$ and its ideal theoretical profile

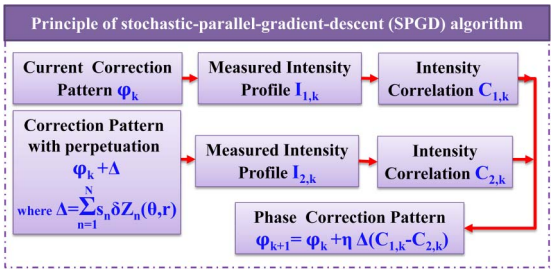

Fig. 2. SPGD algorithm for the $(k+1)$th iteration.

$I_{\mathrm{id}}(r,\theta)$ is then calculated. Next, another phase pattern, $\varphi_k(r,\theta)+\Delta(r,\theta)$, is tried, where

$$\Delta(r,\theta)=\delta\sum_{n=1}^{N}s_nZ_n(r,\theta), \tag{3}$$

with s_n, $n=1,2,\ldots N$, being a random sequence of ± 1 values and δ is a small number, typically ~0.01 (the smaller the better at the expense of longer convergence time). A new measurement of $I_{2,k}(r,\theta)$ is then obtained and a new correlation coefficient $C_{2,k}$ is calculated.

Correction-pattern update: The correction pattern for each iteration is updated using the function $\phi_{k+1}(r,\theta)=\phi_k(r,\theta)+\eta(C_{2,k}-C_{1,k})\Delta(r,\theta)$, where η is an empirically determined constant and which is 200 in our experiment. We note that a smaller η leads to a lower learning rate and a larger η leads to over-correction, both of which tend to decrease the convergence speed. This update for Zernike-polynomial coefficients is thus:

$$\begin{aligned}\varphi_{k+1}(r,\theta)&=\varphi(r,\theta,a_{1,k+1},a_{2,k+1},\ldots,a_{N,k+1})\\ a_{n,k+1}&=a_{n,k}+\eta\delta s_n(C_{2,k}-C_{1,k}),\qquad n=1,2,\ldots,N.\end{aligned} \tag{4}$$

All the Zernike-polynomial terms are updated simultaneously, with the principal update being on the dominant term, i.e., the term causing the largest distortion, while the remaining terms experience random walks (in the "+" or "−" directions) that eventually cancel out.

Figure 3 shows our experimental setup for SPGD phase correction. We first generate a 50-Gbaud QPSK signal at 1550 nm. The signal is then copied into three branches, after being decorrelated by propagation through fibers of different lengths. Collimators at the end of each branch couple the light into free space in the form of three Gaussian beams. These beams are then converted into OAM beams of different orders via spatial light modulators (SLMs) with different phase patterns. One beam [branch (1)] is converted into OAM + 3 for use as the turbulence probe, while the others [branches (2) and (3)] are, respectively, converted into OAM + 1 and OAM + 5. Note that branches (2) and (3) are turned on only when bit-error-rates (BERs) are being measured. After they are combined by the beam splitters, the three beams are transmitted through a turbulence emulator, which is a phase-screen plate that emulates Kolmogorov-spectrum turbulence with an $r_0=1$ mm Fried parameter at 1550 nm [22,25]. Here, we verify

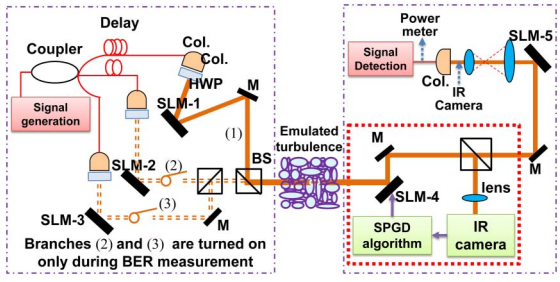

Fig. 3. Experimental setup. Col., collimator; HWP, half-wave plate; SLM, spatial light modulator; M, mirror; BS, beam splitter; IR, infrared.

our approach under static turbulence conditions. However, in a real system, the approach should be: (a) fast enough to track the dynamically varying phase perturbations of the atmospheric turbulence, and (b) able to accommodate any scattering that may cause random power attenuation [7,8]. At the receiver, the intensity profile of the probe beam is recorded by an infrared (IR) camera, providing the feedback signal to the algorithm. The phase-correction pattern, generated by the SPGD algorithm is loaded onto SLM-4 for wavefront restoration of one or more OAM beams. After that, the desired OAM beam is down-converted into a Gaussian-like beam via SLM-5 and then coupled into a single mode fiber for coherent detection.

To monitor the performance of the SPGD-based phase correction, we measured both the far-field intensity profile of each received OAM beam and its interference pattern with a Gaussian beam (before and after phase correction). The Fried parameter of the emulated turbulence is held fixed $r_0 = 1$ mm, and the emulator's phase screen does not rotate during these measurements. Because OAM beams have ℓ-dependent beam diameters, D_ℓ, at the emulator, they thus experience a given turbulence differently. For OAM + 1 to OAM + 5, D_ℓ/r_0 assumes the values 1.5, 1.8, 2.1, 2.4, and 2.7, respectively. We first transmit OAM + 3 through the emulated turbulence and use the SPGD algorithm to generate the phase-correction pattern. This correction pattern is then used to correct the wavefront distortions of a Gaussian beam, as well as those of OAM + 1 to OAM + 5 beams. Figure 4 shows the intensity profiles and interference patterns we obtained for the different OAM beams. Figures 4(b) and 4(e) show that the emulated turbulence distorts both the intensity profile of the OAM beams and the interference patterns. After phase correction, however, both the intensity profiles and the interference patterns indicate that the mode purity is improved [see Figs. 4(c) and 4(f)].

Figure 5(a) shows the intensity correlations of OAM + 3 with and without phase correction for various turbulence realizations under static turbulence conditions ($D_3/r_0 = 2.1$ and $C_n^2 = 3.6 \times 10^{-15}$ m$^{-2/3}$ over an

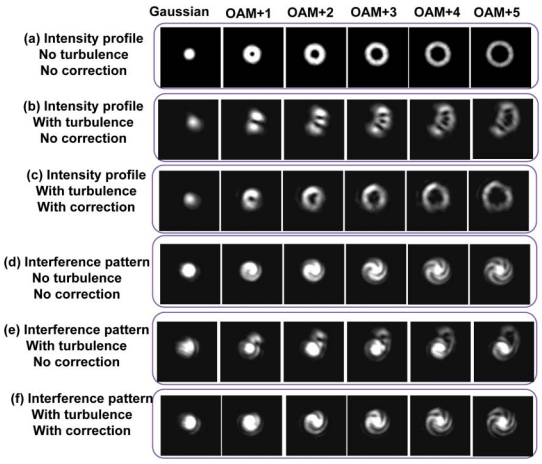

Fig. 4. Far-field intensity profiles and phase interference patterns for various OAM beams before and after phase correction under a specific turbulence realization ($r_0 = 1$ mm). The phase interference patterns are generated by interfering a Gaussian beam with the uncorrected/corrected OAM beams.

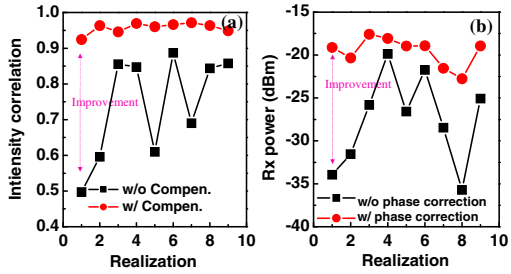

Fig. 5. (a) Intensity correlation and (b) received power of OAM + 3 with and without phase correction when only branch (1) is turned on. We measured nine different realizations with $D_3/r_0 = 2.1$. The iteration numbers for the SPGD algorithm under these nine realizations vary from 56 to 104.

effective path length of 1 km, where C_n^2 is the atmospheric structure constant [26]. Different realizations are obtained by illuminating different regions of the turbulence emulator). The results show that the algorithm improves the beam's intensity correlation to >0.9. Another measure of improvement is the received power coupled into the single-mode fiber. Figure 5(b) shows an increase in the received power on OAM + 3 of 4–15 dB following phase correction.

The convergence speed of an iteration-based phase correction approach is of great importance. Figure 6 shows the intensity correlation and received power for the OAM + 3 probe beam as a function of the algorithm's iteration number. It shows that 50–100 iterations suffice. During a single iteration, the algorithm can only guarantee evaluation of one dominant Zernike-polynomial term. Within 50–100 iterations, all 14 terms could be generated. In addition, the random walks performed by the nondominant terms cancel each other out over 50–100 iterations. To achieve the synchronization among the phase corrector (SLM, 40 Hz refresh frequency), the detector (camera, 50 Hz refresh frequency), and the SPGD algorithm (performed on a personal computer), delays are added among adjacent algorithm stages such that a single iteration takes around 1 s. We believe that faster iteration speed can be achieved with improved hardware and efficient programming.

The turbulence induced wavefront distortion may lead to power leakage from a specific OAM mode to the neighboring modes. As shown in Fig. 7, without phase correction, most of the power of OAM + 3 spreads to its neighboring modes (here, OAM +1 to +5 are measured), and that power distribution approximately uniform distribution. With phase correction, the majority of the power

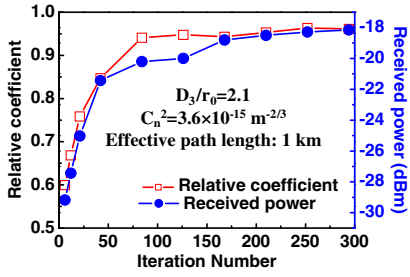

Fig. 6. Intensity correlation and received power as a function of the iteration number (i.e., the number of repetitions that the algorithm loop executed).

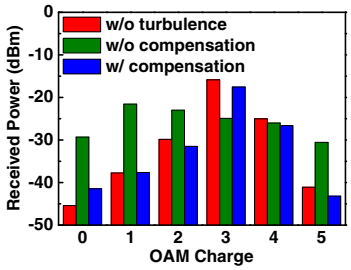

Fig. 7. Received power of various OAM modes before/after phase correction when only OAM + 3 is transmitted. The iteration number for the SPGD algorithm under this turbulence realization is 83.

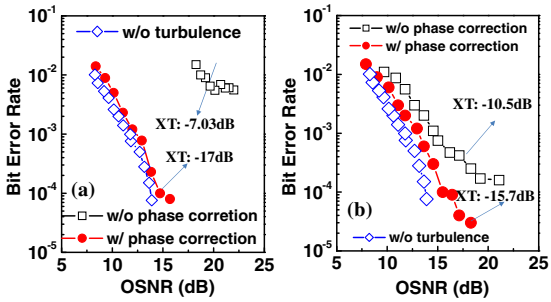

Fig. 8. Measured BERs as functions of optical signal-to-noise ratio (OSNR) when the phase pattern derived from OAM + 3 is used to correct the phases of three simultaneously transmitted OAM beams (OAM + 1, OAM + 3, and OAM + 5). (a) and (b) are two different realizations under the same static turbulence strength. XT: crosstalk. The iteration numbers for the SPGD algorithm under these two turbulence realizations are 76 and 85, respectively.

is concentrated in OAM + 3, with much less power being leaked to the neighboring modes. This implies that our SPGD-algorithm-based phase correction approach reduces the turbulence-induced crosstalk between the OAM channels of a multiplexed communication link.

In a communication system, it is desirable to use a single phase correction for all the channels. To test the capability of SPGD-based wavefront sensing to supply such a phase correction, we applied the correction pattern derived from OAM + 3 to a multiplexed beam, comprising three channels (OAM + 1, +3, and +5), propagating through the same turbulence. Figures 8(a) and 8(b) show the BERs of the OAM + 3 channel before and after phase correction for two turbulence realizations. Without phase correction, the BER can barely reach the forward error correction (FEC) limit of 3.8×10^{-3} [24], because of the large amount of crosstalk from the other two channels. With the phase correction, the BER could achieve the FEC limit.

The following points are worth mentioning: (1) given that our phase correction approach was performed in a lab environment and the turbulence was strong enough to replicate ~1 km of open-air propagation, future implementation of this approach may be applicable in an actual building-to-building or intra-city, link but will require further verification; (2) the proposed method for OAM beam phase correction might be compatible with other schemes, such as a wavefront-sensor-based compensation approach [16].

We thank Jerome Ballesta, Baris Erkman, Prem Kumar, and Tommy Willis for the fruitful discussions. We acknowledge the support of DARPA under the InPho program and Intel Labs University Research Office.

References

1. G. Gibson, J. Courtial, M. Padgett, M. Vasnetsov, V. Pas'ko, S. Barnett, and S. Franke-Arnold, Opt. Express **12**, 5448 (2004).
2. J. Wang, J.-Y. Yang, I. Fazal, N. Ahmed, Y. Yan, H. Huang, Y. Ren, Y. Yue, S. Dolinar, M. Tur, and A. E. Willner, Nat. Photonics **6**, 488 (2012).
3. L. Allen, M. W. Beijersbergen, R. J. C. Spreeuw, and J. P. Woerdman, Phys. Rev. A **45**, 8185 (1992).
4. J. P. Torres and L. Torner, *Twisted Photons: Applications of Light with Orbital Angular Momentum* (Wiley, 2011).
5. A. Mair, A. Vaziri, G. Weihs, and A. Zeilinger, Nature **412**, 313 (2001).
6. H. Hao, G. Xie, Y. Yan, N. Ahmed, Y. Ren, Y. Yue, D. Rogawski, M. J. Willner, B. I. Erkmen, K. M. Birnbaum, S. J. Dolinar, M. P. J. Lavery, M. J. Padgett, M. Tur, and A. E. Willner, Opt. Lett. **39**, 3094 (2014).
7. J. A. Anguita, M. A. Neifeld, and B. V. Vasic, Appl. Opt. **47**, 2414 (2008).
8. N. Chandrasekaran and J. H. Shapiro, J. Lightwave Technol. **32**, 1075 (2014).
9. G. A. Tyler and R. W. Boyd, Opt. Lett. **34**, 142 (2009).
10. K. Murphy, D. Burke, N. Devaney, and C. Dainty, Opt. Express **18**, 15448 (2010).
11. R. W. Boyd, B. Rodenburg, M. Mirhosseini, and S. M. Barnett, Opt. Express **19**, 18310 (2011).
12. I. B. Djordjevic, J. A. Anguita, and B. Vasic, J. Lightwave Technol. **30**, 2846 (2012).
13. T. Weyrauch and M. A. Vorontsov, J. Opt. Fiber Commun. Rep. **1**, 355 (2004).
14. T. Weyrauch and M. A. Vorontsov, Appl. Opt. **44**, 6388 (2005).
15. M. Chen, S. Filippus, and J. Olivier, J. Opt. Soc. Am. A **24**, 1994 (2007).
16. Y. Ren, G. Xie, H. Huang, N. Ahmed, Y. Yan, L. Li, C. Bao, M. P. J. Lavery, M. Tur, M. Neifeld, R. W. Boyd, J. H. Shapiro, and A. E. Willner, Optica **1**, 376 (2014).
17. L. Liu and M. A. Vorontsov, Proc. SPIE **5895**, 138 (2005).
18. S. Zommer, E. N. Ribak, S. G. Lipson, and J. Adler, Opt. Lett. **31**, 939 (2006).
19. G. Xie, Y. Ren, H. Huang, M. P. Lavery, N. Ahmed, Y. Yan, C. Bao, L. Li, Z. Zhao, Y. Cao, M. Willner, M. J. Padgett, M. Tur, S. Dolinar, R. Boyd, J. Shapiro, and A. E. Willner, in *Proceeding Optical Fiber Communication Conference* (IEEE, 2014), paper w1h1.
20. M. Krenn, R. Fickler, M. Fink, J. Handsteiner, M. Malik, T. Scheidl, R. Ursin, and A. Zeilinger, New J. Phys. **16**, 113028 (2014).
21. R. J. Noll, J. Opt. Soc. Am. **66**, 207 (1976).
22. L. C. Andrews and R. L. Phillips, *Laser Beam Propagation through Random Media* (SPIE, 2005).
23. V. N. Mahajan, Opt. Shop Test. **3**, 498 (2007).
24. H. Huang, Y. Ren, Y. Yan, N. Ahmed, Y. Yue, A. Bozovich, B. I. Erkmen, K. Birnbaum, S. Dolinar, M. Tur, and A. E. Willner, Opt. Lett. **38**, 2348 (2013).
25. L. C. Andrews, *Field Guide to Atmospheric Optics*, (SPIE, 2004).
26. ITU-T Recommendation G.975.1, Appendix I.9 (2004).